Manuscript prepared for Atmos. Chem. Phys.
with version 5.0 of the LaTeX class copernicus.cls.
Date: 6 October 2015

A Perturbed Parameter Model Ensemble to Investigate 1991 Mt Pinatubo's Initial Sulfur Mass Emission

Jian-Xiong Sheng[1,*], Debra K. Weisenstein[2], Bei-Ping Luo[1], Eugene Rozanov[1,3], Florian Arfeuille[4,], and Thomas Peter[1]**

[1]Institute for Atmospheric and Climate Science, ETH Zurich, Zurich, Switzerland
[2]School of Engineering and Applied Science, Harvard University, Cambridge, MA, USA
[3]Physikalisch-Meteorologisches Observatorium Davos and World Radiation Center, Davos, Switzerland
[4]Oeschger Centre for Climate Change Research and Institute of Geography, University of Bern, Bern, Switzerland
[*]Now at School of Engineering and Applied Science, Harvard University, Cambridge, MA, USA
[**]Now at Empa, Swiss Federal Laboratories for Materials Testing and Research, Dübendorf, Switzerland

Correspondence to: Jian-Xiong Sheng
(shengj@ethz.ch)

Abstract. We have performed more than 300 atmospheric simulations of the 1991 Pinatubo eruption using the AER 2-D sulfate aerosol model to optimize the initial sulfur mass injection as a function of altitude, which in previous modeling studies has often been chosen in an ad hoc manner (e.g., by applying a rectangular-shaped emission profile). Our simulations are generated by varying a 4-parameter vertical mass distribution, which is determined by a total injection mass and a skew-normal distribution function. Our results suggest that (a) the initial mass loading of the Pinatubo eruption is approximately 14 Mt of SO_2; (b) the injection vertical distribution is strongly skewed towards the lower stratosphere, leading to a peak mass sulfur injection at 18-21 km; (c) the injection magnitude and height affect early southward transport of the volcanic clouds as observed by SAGE II.

1 Introduction

The eruption of Mt Pinatubo on 15 June 1991 injected large amounts of sulfur dioxide into the stratosphere. It perturbed the radiative, dynamical and chemical processes in the Earth's atmosphere (McCormick et al., 1995) and caused a global surface cooling of approximately 0.5 K (Dutton and Christy, 1992). The Pinatubo eruption serves as a useful analogue for geoengineering via injection of sulfur-containing gases into the stratosphere (Crutzen, 2006; Robock et al., 2013). Therefore, modeling volcanic eruptions advances our knowledge not only of the eruptions themselves on weather and climate, but also potential impacts of stratospheric sulfate geoengineering.

The uncertainties in determining the initial total mass and altitude distribution of SO_2 released by Pinatubo remain high. Stowe et al. (1992) deduced a mass of 13.6 megatons of SO_2 based on the aerosol optical thickness observed by the Advanced Very High Resolution Radiometer (AVHRR). By analyzing SO_2 absorption measurements from the Total Ozone Mapping Spectrometer (TOMS) satellite instrument, Bluth et al. (1992) estimated an initial mass loading of approximately 20 Mt of SO_2. This study was later reevaluated by Krueger et al. (1995), who determined a range of 14-28 Mt emitted by Pinatubo, given the large retrieval uncertainties associated with TOMS. Later, Guo et al. (2004) constrained this range to 14-22 Mt of SO_2. Besides the total emitted mass, the altitude distribution of the SO_2 emission is also not well constrained. The only available measurements with vertical resolution of SO_2 in the stratosphere during the Pinatubo period have been made by the Microwave Limb Sounder (MLS) in September 1991 (Read et al., 1993), which unfortunately only started its mission three months after the eruption. Given the lack of measurements in the period immediately following the Pinatubo eruption, modeling studies of Pinatubo (e.g., Weisenstein et al., 1997; Timmreck et al., 1999; SPARC, 2006; Heckendorn et al., 2009; Niemeier et al., 2009; Toohey et al., 2011; Aquila et al., 2012; English et al., 2013; Dhomse et al., 2014) have employed very different mass loadings, emission altitudes and vertical mass distributions, which leads to biases in the local heating

and consequently in the dynamical response and time evolution of the stratospheric aerosol burden. These uncertainties, in addition to model-specific artifacts, make it difficult to accurately simulate the Pinatubo eruption.

Here, we attempt to provide a solution to the problems outlined above. We use the AER 2-D size-bin resolving (also called sectional or spectral) sulfate aerosol model (Weisenstein et al., 1997), which participated in an international aerosol assessment (SPARC, 2006), and was one of the best-performing stratospheric aerosol models (in terms of comparing SO_2, aerosol size distributions and extinctions with observations) under both background and volcanic conditions. We present results from more than 300 atmospheric simulations of the Pinatubo eruption based on different combinations of four emission parameters, namely the total SO_2 mass and a 3-parameter skew-normal distribution of SO_2 as a function of altitude. We calculate aerosol extinctions from all of the simulations and compare them with Stratospheric Aerosol and Gas Experiment II (SAGE II) measurements (Thomason et al., 1997, 2008). Such a head-on approach is currently impossible for global 3-D models due to computational expenses. The purpose of this work is to provide a universal emission scenario for global 3-D model simulations. To this end we optimize the emission parameters such that the resulting SO_2 plume, aerosol size distributions, aerosol burdens and extinctions match balloon-borne, satellite and lidar measurements. We repeat two simulations using the 3-D SOCOL-AER aerosol-chemistry-climate model (Sheng et al., 2015) as a consistency check in a more complex model. In Section 2 we describe the model and the experimental design of our Pinatubo simulations. Section 3 compares the Pinatubo simulations with the observations, and conclusions follow in Section 4.

2 Method

2.1 AER 2-D sulfate aerosol model

The AER 2-D sulfate aerosol model participated in an international aerosol assessment (SPARC, 2006), in which it was compared with satellite, ground lidar and balloon measurements, as well as with other 2-D and 3-D aerosol models, and subsequently recognized as one of the best existing stratospheric aerosol models with respect to SO_2, aerosol size distributions and extinctions under both background and volcanic conditions. The model represents sulfuric acid aerosols (H_2SO_4/H_2O) on the global domain from the surface to about 60 km with approximately 9.5° horizontal and 1.2 km vertical resolution. The model is driven by year-by-year wind fields and temperature from Fleming et al. (1999), which were derived from observed ozone, water vapor, zonal wind, temperature, planetary waves, and quasi-biennial oscillation (QBO). The model chemistry includes the sulfate precursor gases carbonyl sulfide (OCS), sulfur dioxide (SO_2), sulfur trioxide (SO_3), sulfuric acid (H_2SO_4), dimethyl sulfide (DMS), carbon disulfide (CS_2), hydrogen sulfide (H_2S) and methyl sulfonic acid (MSA). The model uses pre-calculated values of OH and other oxidants from Notholt et al. (2005). Photodissociation and chemical reactions are listed in Weisenstein et al. (1997) and their rates are updated to Sander et al. (2011). The particle distribution is resolved by 40 size bins spanning wet radii from 0.39 nm to 3.2 μm by volume doubling. Such a sectional approach was proven to be more accurate in representing aerosol mass/extinctions compared to prescribed unimodal or multimodal lognormal distributions (Weisenstein et al., 2007). The sulfuric acid aerosols are treated as liquid binary solution droplets. Their exact composition is directly derived from the surrounding temperature and humidity according to Tabazadeh et al. (1997). Microphysical processes in the model include homogeneous nucleation, condensation/evaporation, coagulation, sedimentation, as well as tropospheric rainout/washout. These processes determine the evolution of the aerosol concentration in each size bin, thus the entire particle size distribution. Operator splitting methods are used in the model with a time step of one hour for transport, chemistry, and microphysics, and 3-minute substeps for the microphysical processes that exchange gas-phase H_2SO_4 with condensed phase, and 15-minute substeps for the coagulation process. For more detailed descriptions of chemistry and microphysics in the model we refer to Weisenstein et al. (1997, 2007).

2.2 Coupled 3-D aerosol-chemistry-climate model

We employ the coupled aerosol-chemistry-climate model SOCOL-AER (Sheng et al., 2015) in order to verify the consistency between a 2-D model forced with observed dynamics and a 3-D free-running model. SOCOL-AER couples the size resolved AER 2-D microphysical model into the chemistry-climate model SOCOL (Stenke et al., 2013) with interactive aerosol radiative forcing. In this study we use the T31 horizontal resolution (3.75°×3.75°) and 39 vertical levels (from surface to 0.01 hPa) with nudged quasi-biennial oscillation. Transport is calculated every 15 minutes, whereas chemistry, microphysics and radiation are calculated every two hours with 40 substeps (3-minute) for the microphysics. This model has been well validated by comparing calculations with sulfur-containing gases, aerosol extinctions at different wavelength channels (from 525 nm to 5.26 μm), and aerosol size distributions from satellite and in situ observations. It has been used to study the global atmospheric sulfur budget under volcanically quiescent conditions and moderate volcanic eruptions such as the 2011 Nabro eruption. A detailed description of SOCOL-AER is presented by Sheng et al. (2015).

Table 1. Scores and rankings of 326 AER 2-D atmospheric simulations of the Pinatubo eruption sorted according to the weighted rank ("RankWt"). The weighting is given by 16.7% of the SO_2 score (ScoreSO_2), 16.7% of the OPC score (ScoreOPC), 33.3% of the global burden score (ScoreBurden), and 33.3% of the aerosol extinction score (ScoreExt). The rank computed by the arithmetic average of the four scores is also provided ("RankAvg"). Scores of two additional 3-D simulations "R001 3-D" and "R153 3-D" from the aerosol-chemistry-climate model SOCOL-AER are provided at the bottom of the table.

Mass (Mt SO_2)	Location μ (km)	Scale σ (km)	Skewness α	Score SO_2	Score OPC	Score Burden	Score Ext	Score Avg	Score Wt	Rank SO_2	Rank OPC	Rank Burden	Rank Ext	Rank Avg	Rank Wt	Scenario Name
14	22.59	4	-2	0.22	0.47	0.16	0.22	0.27	0.24	20	23	7	10	2	1	R001
14	22.59	3	-2	0.11	0.47	0.19	0.25	0.26	0.25	4	24	14	30	1	2	
14	20.27	2	0	0.19	0.47	0.19	0.24	0.27	0.25	14	21	11	25	3	3	
14	21.43	3	-1	0.28	0.47	0.17	0.22	0.28	0.25	29	22	8	11	5	4	
14	21.43	4	-1	0.35	0.50	0.14	0.20	0.30	0.25	52	46	2	3	7	5	
14	19.11	3	0	0.38	0.48	0.15	0.20	0.30	0.26	57	32	4	5	8	6	
14	21.43	2	-1	0.19	0.45	0.21	0.26	0.28	0.26	13	13	19	33	4	7	
14	17.95	4	0	0.44	0.50	0.13	0.19	0.32	0.26	72	49	1	2	15	8	R008
14	20.27	3	0	0.31	0.53	0.17	0.21	0.30	0.27	42	67	9	7	9	9	
14	19.11	4	0	0.41	0.54	0.14	0.19	0.32	0.27	68	77	3	1	18	10	R010
14	22.59	3	-1	0.22	0.52	0.21	0.24	0.30	0.27	18	65	20	20	6	11	
14	20.27	4	-1	0.45	0.46	0.16	0.21	0.32	0.28	77	17	6	9	22	12	
14	21.43	4	-2	0.40	0.45	0.19	0.23	0.32	0.28	64	8	12	14	16	13	
14	22.59	4	-1	0.34	0.54	0.19	0.21	0.32	0.28	51	88	13	8	19	14	
14	16.79	4	0	0.50	0.48	0.15	0.20	0.33	0.28	88	29	5	4	26	15	
14	21.43	3	-2	0.37	0.44	0.21	0.24	0.31	0.28	54	3	18	28	14	16	
14	21.43	2	-2	0.28	0.43	0.24	0.27	0.31	0.29	31	1	28	53	10	17	R017
14	23.75	4	-2	0.29	0.54	0.22	0.24	0.32	0.29	36	81	24	18	21	18	
14	21.43	2	0	0.20	0.53	0.25	0.27	0.31	0.29	16	69	35	46	11	19	
14	17.95	3	0	0.51	0.46	0.18	0.22	0.34	0.30	89	16	10	13	32	20	
...	...	...														
14	22.59	2	-2	0.34	0.47	0.23	0.29	0.33	0.31	49	20	26	72	27	32	
17	22.59	4	-2	0.07	0.55	0.31	0.32	0.31	0.31	3	96	63	103	13	33	R033
17	21.43	4	-1	0.23	0.57	0.28	0.27	0.34	0.32	23	105	48	50	29	34	
...	...	...														
17	22.59	3	-1	0.21	0.60	0.40	0.38	0.40	0.40	17	126	124	151	66	84	
14	22.59	2	0	0.54	0.60	0.34	0.29	0.44	0.40	95	120	81	73	91	85	
20	21.43	3	-1	0.04	0.62	0.44	0.45	0.39	0.40	1	142	154	180	58	86	R086
17	23.75	4	-2	0.30	0.62	0.42	0.39	0.43	0.42	39	140	138	155	86	99	
20	19.11	4	-2	0.71	0.52	0.36	0.30	0.47	0.42	135	62	96	86	105	100	
14	/	/	/	0.70	0.70	0.31	0.26	0.49	0.43	133	184	66	36	119	101	Box14Mt
17	17.95	3	-1	0.77	0.49	0.34	0.32	0.48	0.43	151	38	82	100	110	102	
...	...	...														
14	26.07	3	-1	0.94	0.71	0.43	0.32	0.60	0.53	197	195	141	104	167	153	R153
...	...	...														
17	16.79	3	-2	0.96	0.61	0.55	0.54	0.67	0.63	204	138	204	224	200	213	
20	/	/	/	0.47	0.78	0.67	0.59	0.63	0.63	79	244	249	241	178	214	SPARC20Mt
20	21.43	3	0	0.48	0.75	0.66	0.62	0.63	0.63	82	220	242	251	177	215	
...	...	...														
20	29.55	3	-1	1.46	0.92	0.92	0.95	1.06	1.02	307	310	313	320	320	322	
20	28.39	3	0	1.42	0.93	0.93	0.96	1.06	1.02	301	312	315	324	319	323	
20	28.39	2	0	1.60	0.88	0.89	0.94	1.08	1.02	320	298	298	317	322	324	
20	29.55	2	-1	1.67	0.86	0.88	0.93	1.08	1.02	321	288	297	313	326	325	
20	29.55	3	0	1.52	0.90	0.91	0.95	1.07	1.02	317	306	306	322	321	326	
14	∼22	4	-2	0.30	0.46	0.18	0.20	0.29	0.25							R001 3-D
14	∼26	3	-1	0.93	0.53	0.36	0.38	0.55	0.49							R153 3-D

2.3 Experiments

We have simulated the Pinatubo-like eruption by injecting SO_2 directly into the stratosphere. In the 2-D model, the injection is immediately mixed zonally, and takes place into the latitude band 5°S–14°N, which is an approximation to the observed rapid zonal transport of the SO_2 cloud derived from satellite measurements (Bluth et al., 1992; Guo et al., 2004). The lack of zonal resolution is clearly a deficiency of our approach, but since SO_2 removal/conversion rate (e-folding time) is sufficiently slow ($\tau \sim 25$ days) and the zonal transport around the globe sufficiently fast ($\tau \sim 20$ days) (Guo et al., 2004), a zonal-mean description is a reasonable approximation. Also, the spaceborne aerosol data are typically provided as zonal averages. We examined three cases of total mass, namely 14, 17 and 20 Mt of SO_2. The injection height extends from near the tropical tropopause (17 km) to 30 km. The vertical mass distribution is then represented by $M_{tot}F(z)$ where M_{tot} is the SO_2 mass magnitude in units of megaton (Mt) and $F(z) = f(z)/\int_{z_{\min}=17}^{z_{\max}=30} f(x)\,\mathrm{d}x$ (in km^{-1}) is a vertical distribution function of altitude $z \in [17\,\mathrm{km}, 30\,\mathrm{km}]$ with a skew-normal distribution $f(z)$ given

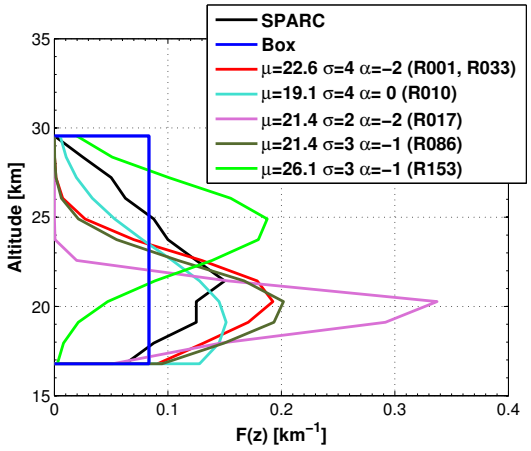

Fig. 1. Vertical distribution function $F(z)$. Black line: used in SPARC (2006) Blue line: uniform (box) profile that distributes SO_2 homogeneously with altitudes. Each of these curves encloses a unit area.

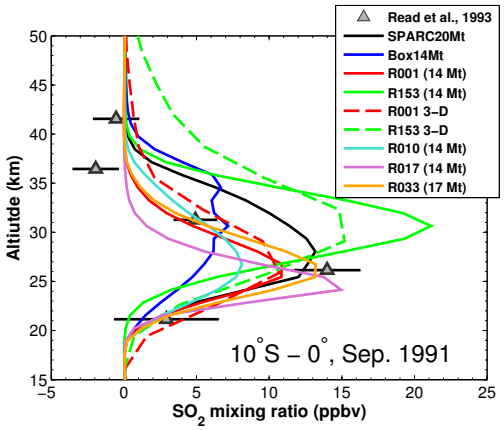

Fig. 2. Vertical profiles of monthly zonal mean SO_2 mixing ratio at 10°S-0°N in September 1991. Different simulations are represented in different colors. Observations (triangles) are taken from Microwave Limb Sounder (MLS) measurements (Read et al., 1993).

by (Azzalini, 2005)

$$f(z) = \frac{2}{\sqrt{2\pi}\sigma} e^{-\frac{(z-\mu)^2}{2\sigma^2}} \int_{-\infty}^{\alpha\frac{z-\mu}{\sigma}} \frac{1}{\sqrt{2\pi}} e^{-\frac{x^2}{2}}\, \mathrm{d}x$$

Figure 1 shows a few examples of $F(z)$. The location parameter μ depends on available model levels and determines the altitude where the maximum of the emitted SO_2 cloud is located when there is no skewness. The skewness or asymmetry of the curve increases when $|\alpha|$ increases and vanishes when $\alpha = 0$ (normal distribution). A negative α drives the location of the maximum SO_2 emission to lower altitudes, while a positive α to higher altitudes. The scale parameter σ indicates how much dispersion takes place near the maximum, that is, it determines the width or standard deviation of the asymmetric bell-shaped curve.

The four parameters M_{tot}, μ, σ and α enable representation of a substantial space of SO_2 distributions, whose evolution is computed forward in time (taking into account the transport and comprehensive chemical and microphysical processes), in order to compare with the satellite extinction data. We simulate the following cases in detail:

$$M_{tot} \in \{14\,\mathrm{Mt}, 17\,\mathrm{Mt}, 20\,\mathrm{Mt}\},$$

$$\mu \in \{16.79\,\mathrm{km} + n \times 1.16\,\mathrm{km}, n = 0 \ldots 11\},$$

$$\sigma \in \{2\,\mathrm{km}, 3\,\mathrm{km}, 4\,\mathrm{km}\}$$

$$\alpha \in \{-2, -1, 0\}$$

which results in 324 different scenarios. The choice of the boundaries for this set of scenarios is already based on exploratory simulations. For example, based on the results of our 2-D model, it does not make sense to consider total masses $M_{tot} > 20$ Mt, since no choice of the other three parameters would allow to reconcile the model results with the observations. Similarly, skewness $\alpha > 0$ leads to more biased model results, because the skew towards higher altitudes cannot be offset by lower M_{tot}. In addition to the above 324 simulations, we consider another two scenarios, which are adopted in modeling studies of Pinatubo: (1) Box14Mt has a uniform ('Box') profile, which is similar to Dhomse et al. (2014) and the simulation "CONTROL_HIGH" in Aquila et al. (2012), injecting the SO_2 mass homogeneously along altitudes (shown in Figure 1); (2) SPARC20Mt is the reproduction of the Pinatubo simulation conducted in SPARC (2006), which injects 20 Mt of SO_2 and has a vertical profile 'SPARC' shown in Figure 1.

A selected list from the 326 2-D simulations is summarized in Table 1, in which the specific choice of the four parameters for each scenario is provided. The score and ranking of these scenarios are discussed later in the text.

Given the limitation of the 2-D approach, we further perform two 3-D Pinatubo-like simulations (R001 3-D and R153 3-D at the bottom of Table 1) using the coupled aerosol-chemistry-climate model SOCOL-AER Sheng et al. (2015) to check the consistency between 2-D and 3-D approaches. Note that the location parameters used in the 3-D runs differ slightly from the corresponding 2-D runs (i.e. R001 and R153) due to different vertical model levels between the two models.

3 Results and Discussions

We compare our results with SO_2 vertical profiles measured by the Microwave Limb Sounder (MLS) onboard the Upper Atmosphere Research Satellite (UARS) between 10°S-0° in September 1991 (Read et al., 1993), the optical par-

ticle counter (OPC) measurements operated above Laramie, Wyoming (Deshler et al., 2003; Deshler, 2008), the global aerosol burden derived from the High-resolution Infrared Radiation Sounder (HIRS) (Baran and Foot, 1994) and from Stratospheric Aerosol and Gas Experiment II (SAGE II) using the 4λ method (SAGE-4λ) (Arfeuille et al., 2013; Luo, 2015), as well as aerosol extinctions measured by SAGE II (Thomason et al., 1997, 2008).

3.1 Metrics and data sets

To determine an optimal set of the emission parameters, we define four metrics (ScoreSO_2, ScoreBurden, ScoreOPC and ScoreExt) based on these four measurements sets described above, and rank all of our 326 simulations by a weighted score (ScoreWt) of the four metrics (see Table 1).

ScoreSO_2 is calculated as the relative l^2-norm (Euclidean norm) error with respect to the MLS measurements:

$$||X_{\mathrm{SO_2,model}} - X_{\mathrm{SO_2,MLS}}||/||X_{\mathrm{SO_2,MLS}}||,$$

where X is a one-dimensional vector of SO_2 mixing ratio in altitude (21 km, 26 km, 31 km, 36 km and 41 km). The negative values of the MLS measurements are set to zero in the calculation.

ScoreBurden is the average of the relative l^2-norm errors with respect to HIRS (Jul. - Dec. 1991) and SAGE-4λ (Jan. 1992 - Dec. 1993):

$$\frac{1}{2}(||B^{t_1}_{\mathrm{model}} - B^{t_1}_{\mathrm{HIRS}}||/||B^{t_1}_{\mathrm{HIRS}}|| + ||B^{t_2}_{\mathrm{model}} - B^{t_2}_{\mathrm{SAGE}}||/||B^{t_2}_{\mathrm{SAGE}}||)$$

where B^{t_1} is a one-dimensional (in time) vector of the aerosol burden for Jul. - Dec. 1991 and B^{t_2} for Jan. 1992 - Dec.1993.

ScoreOPC. We first calculate the relative l^2-norm errors with respect to the OPC measurements:

$$\mathrm{errOPC} = ||N_{\mathrm{model}} - N_{\mathrm{OPC}}||/||N_{\mathrm{OPC}}||$$

where N is a one-dimensional vector of the cumulative particle number concentration in altitude (15-30 km). We then evaluate a quadratic mean (RMS):

$$\mathrm{rmsOPC} = \mathrm{RMS}\{\mathrm{errOPC}_r\}$$

where r denotes four particle size channels ($r > 0.01\,\mu$m, $r > 0.15\,\mu$m, $r > 0.25\,\mu$m and $r > 0.5\,\mu$m). Finally, ScoreOPC is obtained by averaging rmsOPC from October 1991 to December 1992.

ScoreExt. The uncertainty of SAGE is generally better than $\sim$20% for 525 nm and $\sim$10% for 1020 nm (see Fig. 4.1 in SPARC (2006)). Therefore, ScoreExt is weighted as one third for 525 nm (ScoreExt525nm) and two thirds for 1020 nm (ScoreExt1020nm). We use the SAGE II observations between 18 and 30 km. The calculations for ScoreExt525nm and ScoreExt1020nm are similar to those in ScoreOPC. Latitude bands (50-40°S, 30-20°S, 5°S-5°N, 20-30°N and 40-50°N) take the place of the particle size channels. The temporal average is from January 1992 to December 1993.

Note that extinction coefficients in the lower stratosphere (18-23km) have a much larger weight than those above 23 km because extinctions at 525 nm and 1020 nm at 18-23 km after the Pinatubo eruption (see Figure 5) are one to several orders of magnitude larger than those above 23 km. We calculate the score by the relative Euclidean norm, therefore the scores above 23 km have a relatively small weight.

The overall score ScoreWt is weighted as follows: 16.7% of the SO_2 score (ScoreSO_2), 16.7% of the OPC score (ScoreOPC), 33.3% of the global burden score (ScoreBurden), and 33.3% of the aerosol extinction score (ScoreExt). The choice of the weighting is discussed below.

MLS detected residual SO_2 in the stratosphere approximately 100 days after the eruption. The uncertainty of ScoreSO_2 is likely larger than ScoreBurden and ScoreExt due to uncertain OH fields. Assuming an uncertainty in OH fields of 10% (e.g., Prinn et al., 2005) translates into an uncertainty of 30% in SO_2 at $\sim$90 days after the eruption. Moreover, ScoreOPC has also less weight than ScoreBurden and ScoreExt because of the small temporal and spatial sample size of the ballon-borne OPC measurements, which are not conducted very frequently (a maximum of two measurements per month after the Pinatubo eruption) and located only above Laramie.

ScoreBurden uses the HIRS-derived data up to December 1991 and the SAGE-derived data afterwards. During the first 6 months after the Pinatubo eruption, the SAGE II instrument was largely saturated in the tropical region (Russell et al., 1996; Thomason et al., 1997; SPARC, 2006; Arfeuille et al., 2013), and therefore the aerosol mass retrieved from SAGE II during this period very likely underestimates the initial loading significantly. The SAGE-4λ data set corrects for this deficiency by filling observational gaps by means of Lidar data. However, Lidar-derived extinctions are generally lower than SAGE II below 21 km (SPARC, 2006), and are not located in the equatorial region (see Fig. 3.7 in SPARC (2006)), where maximum mass loadings are expected. Therefore, SAGE II gap-filled data probably remain as a lower limit after the eruption. Conversely, HIRS measurements represent an upper limit since they account for the entire aerosol column including the troposphere. This may explain the considerable difference between SAGE II and HIRS during the first six months after Pinatubo (see Figure 3). After this period, the aerosol mass in the extratropics contributes more to the global value than that in the tropics because the volcanic cloud starts to spread out from the tropics in November 1991 (see Fig. 5 of Baran and Foot (1994)). HIRS loses its sensitivity at mid/high latitudes where there is a contribution from errors in the background signal (Baran and Foot, 1994). As shown in Figure 3, a visible increase of the HIRS-derived global burden begins after December 1991, and the noises in

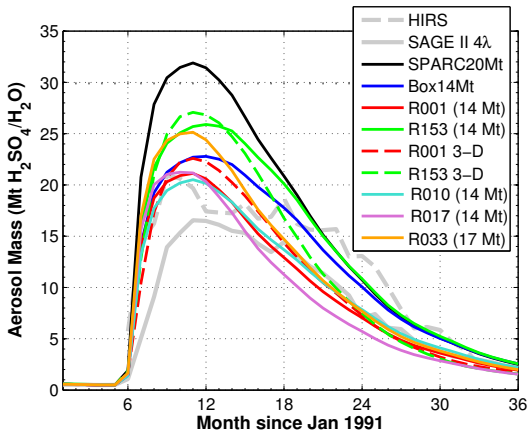

Fig. 3. Evolution of simulated global stratospheric aerosol burden (Mt H_2SO_4/H_2O) compared to the HIRS and SAGE II-derived data. HIRS-derived data include both tropospheric and stratospheric aerosols (Baran and Foot, 1994). SAGE II aerosol data is derived from the retrieval algorithm SAGE 4λ by Arfeuille et al. (2013), and includes only stratospheric aerosols.

HIRS become more pronounced after March 1992. On the other hand, SAGE II, as an occultation instrument, becomes more reliable when the stratosphere starts to be sufficiently transparent after December 1991, particularly in mid latitudes. Therefore, ScoreBurden uses the HIRS-derived data up to December 1991 and the SAGE-derived data afterwards, with an overall uncertainty of 20%. ScoreExt uses the SAGE II measurements from January 1992 to exclude the most saturated phase of SAGE II.

3.2 Scoring table

Table 1 shows the scores of selected scenarios, sorted according to the weighted rank ("RankWt" in the next to last column). The rank computed by the arithmetic average of the four scores is also provided ("RankAvg" in the third column from the right). The top 20 scenarios reveal that the total injection mass (M_{tot}) is 14 Mt of SO_2, 70-80% of which is below 24 km, and its maximum is likely between 18-21 km with 3-4 km width (scale parameter σ). Location parameters μ larger than 21 km are skewed towards a lower altitude (negative α). These sort of vertical profiles provide a range for the parameters of the optimal vertical distribution: $\mu = 20.66 \pm 1.79$ km, $\sigma = 3.33 \pm 0.72$ km and $\alpha = -0.8 \mp 0.77$. Two examples (scenarios R001 and R010 marked in Table 1) are shown in Figure 1. The ranking based on "RankAvg" slightly differs from "RankWt", however the set of the best scenarios found in "RankAvg" is consistent with "RankWt" despite the distinct weighting schemes. The worst scenarios ("RankWt" $\geq$322) in Table 1 are those with 20 Mt SO_2 injection mass and highest location parameters ($\mu = 29.55$ km). The scenarios such as Box14Mt and R153 rank much more poorly than the optimal scenarios, although their injection mass is the same, because their vertical profiles (shown in Figure 1) inject over 50% mass above 23-24 km. The scenario R033 has the same vertical profile as R001, but injects 17 Mt SO_2. SPARC20Mt emits 20 Mt SO_2 and ranks at 214 in Table 1, although its vertical profile is close to the optimal scenarios (about 10-20% more mass above 23 km). This implies that emitting above 17 Mt SO_2 is very likely an overestimation.

The optimal vertical profiles found in Table 1 are generally consistent with the earlier volcanic plume studies of Fero et al. (2009) and Herzog and Graf (2010). Fero et al. (2009) showed that the SO_2 plume from the 1991 Pinatubo eruption originated at an altitude of $\sim$25 km near the source and descended to an altitude of $\sim$22 km as the plume moved across the Indian Ocean. Herzog and Graf (2010) suggested that initially SO_2 from a co-ignimbrite eruption (such as Pinatubo) that was forced over a large area, may reach above 30 km but the majority of SO_2 would then collapse or sink back to its neutral buoyancy height (15-22 km) (see Fig.1 in their paper).

We discuss in detail nine scenarios (R001, R010, R017, R033, R153, Box14Mt, SPARC20Mt, R001 3-D and R153 3-D). R001 represents the overall optimal scenario. R010 ranks first in the ScoreExt and third in the ScoreBurden, as an example of scenarios with high rankings in the extinction and aerosol burden scores. R017 matches best the OPC measurement, but has poorer scores in the other criteria than R001 and R010. R086 has a vertical profile similar to R001 (see Figure 1), and agrees the best with the SO_2 observations. However, this scenario fails to match other observations due to its abundant initial injection of 20 Mt SO_2. R033 emitted 17 Mt SO_2 with the same vertical profile of R001, and ranks third in the ScoreSO_2 but poorly among other scores, which shows a performance similar to R086. Here we will focus on R033 for later discussion. R153 and Box14Mt (with RankWt 94) inject the same sulfur mass as in R001, but use different vertical profiles (maximum injection mass of R153 is located at $\sim$26 km). SPARC20Mt turns out to be a bad representation, which reproduces the previous simulation conducted in SPARC (2006). The two 3-D scenarios R001 3-D and R153 3-D correspond to the 2-D scenarios R001 and R153, respectively. The scores of the 3-D runs are similar to the corresponding 2-D ones.

3.3 Matching SO_2

Figure 2 compares the modeled SO_2 with MLS measurements in September 1991. The scenario R001 captures the measured SO_2 profile, and only underestimates the measured maximum SO_2 mixing ratio near 26 km by about 20%. SO_2 modeled by R033 agrees excellently (within 7%) with MLS measurement. R010 produces about 20-30% less SO_2 near 26 km compared to R001, and rather more above 30 km. This could be explained by the fact that R010 disperses slightly more SO_2 above 24 km compared to R001. The SO_2 ver-

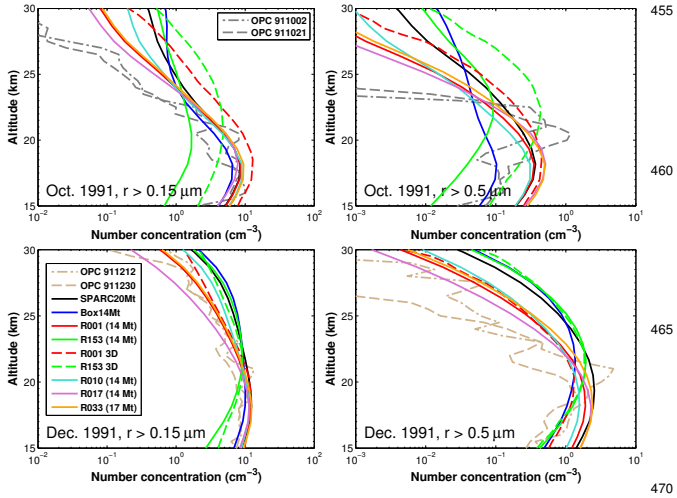

Fig. 4. Cumulative particle number concentrations of OPC measurements (Deshler et al., 2003; Deshler, 2008), and model simulations in October 1991 (upper panels) and December 1991 (lower panels) for particle size channels $r > 0.15\,\mu$m (left panels) and $r > 0.5\,\mu$m (right panels).

tical profile of R017 is shifted to lower altitudes compared with the observed values, likely due to its concentrated injection distribution near 19-20 km (see Figure 1). Box14Mt and R153 fail to match the observed profile. SPARC20Mt agrees with the observations under 28 km better than Box14Mt and R153, but largely overestimates the observations above. The common feature of R153, Box14Mt and SPARC20Mt is that their initial vertical distributions release much more SO_2 above 24 km compared to R001, which is skewed towards lower altitudes, therefore retaining more than 90% of emitted SO_2 below 24 km (Figure 1). SO_2 profiles simulated by the two 3-D simulations (dashed curves in Figure 2) are similar to the corresponding AER 2-D results, though SOCOL-AER predicts a lower maximum value and more readily distributes SO_2 to higher altitudes, reflecting differences in OH and transport between the two models.

3.4 Matching the burden

Figure 3 shows the evolution of the simulated stratospheric aerosol burden (megaton of H_2SO_4/H_2O) compared to that derived from HIRS (Baran and Foot, 1994) and SAGE-4λ (Arfeuille et al., 2013). R001 matches the HIRS-derived maximum aerosol burden of 21 Mt (equivalently 15-16 Mt of sulfate mass without water) during the first few months after the eruption, and after month 14 agrees with the SAGE-derived burden (mostly within 20%). In contrast, SPARC20Mt reaches a maximum burden of 32 Mt of H_2SO_4/H_2O, which is ∼50% more than the 21 Mt derived from HIRS. R033 emits 17 Mt of SO_2 using the same vertical profile as R001, and peaks at 25 Mt of aerosol mass, about ∼30% more than HIRS, whereas the uncertainty of HIRS is about 10% (Baran and Foot, 1994). This means that the initial mass loading of 17 or 20 Mt of SO_2 into the stratosphere is apparently too high. Scenarios using 14 Mt of SO_2 show that the evolution of the aerosol burden is highly sensitive to different injection profiles. R010 initially distributes somewhat more SO_2 above 24 km compared to R001, and shows a better decay rate of the aerosol burden. R017 emits SO_2 mainly concentrated between 19-21 km, and its aerosol burden peaks similarly to R001, but declines more rapidly. R153 and Box14Mt inject about 60% and 40% of their sulfur mass above 24 km, respectively, leading to a greater maximum aerosol burden and a slower decay rate of the burden than R001. R153 has even a slightly larger maximum aerosol burden than R033, though R033 has the larger initial SO_2 mass loading. Together, these results reveal that the injection altitude and initial mass loading affect the lifetime of the volcanic aerosol. An increase in the distance of the volcanic plume above the tropopause will increase the lifetime of the volcanic aerosol due to a longer residence time for sedimenting particles and a slower pathway of the aerosol within the Brewer-Dobson circulation. On the contrary, a larger initial mass loading may offset a higher injection altitude because of faster sedimentation caused by larger particles.

The results of "R001 3-D" using the coupled aerosol-chemistry-climate model SOCOL-AER is consistent (mostly within 10%) with the AER 2-D simulation R001. In contrast, the consistency between R153 and "R153 3-D" is less satisfactory. The maximum aerosol burden simulated by "R153 3-D" is within 10% of R153, but the e-folding time of the aerosol burden in the 3-D simulation ("R153 3-D") is significantly faster (13 versus 15 months) than in the 2-D simulation (R153). This indicates that in addition to the initial mass loading and microphysics, model dynamics is essential to the decay of the volcanic aerosols. This difference between R153 (AER) and "R153 3-D" (SOCOL-AER) is possibly due to an insufficient rate of exchange of air between the troposphere and stratosphere in the AER 2-D model (Weisenstein et al., 1997) and/or a faster Brewer-Dobson circulation with respect to observations in the SOCOL (see the "tape recorder" in Fig. 8 of Stenke et al. (2013)).

3.5 Matching particle size distributions

Figure 4 shows comparisons between the optical particle counter (OPC) measurements operated above Laramie (Deshler et al., 2003; Deshler, 2008) and model-calculated cumulative particle number concentrations in October and December 1991 for two size channels ($r > 0.15\,\mu$m and $r > 0.5\,\mu$m). Below 23 km, R001 reasonably matches the observations for $r > 0.15\,\mu$m, but less satisfactorily for $r > 0.5\,\mu$m. The number density from R010 is slightly higher than R001 above ∼24 km, which is consistent with the comparison between initial vertical profiles of R001 and R010 (see Figure 1). R017 agrees best with the observed number density, particularly above 24 km, because R017 emits very

little SO_2 above 22 km. R033 predicts slightly higher number concentrations than R001 due to its larger initial mass loading (17 Mt SO_2), but shows in general similar results to R001. In contrast, the calculations from R153, Box14Mt and SPARC20Mt differ significantly from R001. Above 23 km, these three scenarios further overestimate the observations than R001 because their initial injection profiles release much more SO_2 above 23 km compared to R001. Below 23 km, R153 substantially underestimates the observations in October 1991 as its injected mass locates mainly between 23-27 km, while Box14Mt shows better agreement with the observations ($r > 0.5\,\mu$m) below 18 km than R001, but largely underestimates the maximum near 21 km. SPARC20Mt is similar to R001 below 20 km since its initial mass loading (20 Mt SO_2) compensates for the deficiency of its vertical mass injection profile in the lower stratosphere. The calculations from SOCOL-AER are generally consistent with the corresponding 2-D ones (R001 and R153). SOCOL-AER produces higher number concentration in October 1991 compared to the AER 2-D model. In December 1991 this difference between the 2-D and 3-D simulations shrinks, and "R001 3-D" further improves the agreement with the OPC measurements below 18 km for $r > 0.5\,\mu$m.

3.6 Matching extinctions

We compare the modeled 1020 nm extinctions with the gap-filled SAGE II version 7.0 (Figure 5). SAGE II data points with horizontal bars are actual SAGE II measurements and denote natural variabilities, while data points without bars are gap-filled from lidar ground stations, which have a higher uncertainty (SPARC, 2006). Figure 5 shows comparisons in January (upper panel) and July (lower pannel) 1992 for five latitude bands from left to right: 50-40°S, 30-20°S, 5°S-5°N, 20-30°N and 40-50°N.

In January 1992, all the simulations reproduce aerosol extinctions reasonably near 20 km (mostly within 50-100% of observed aerosol extinctions). R001, R010 and R017 agree better with observed aerosol extinctions compared to the other 2-D simulations. R010 performs best in the lower stratosphere (where ScoreExt by definition has a large weight), while R017 matches the observations well above 24 km. R033 is generally 10-20% larger than R001 due to its higher initial mass loading, although it has the same vertical profile as R001. SPARC20Mt has even larger values than R033 due to a 20 Mt of SO_2 mass loading. Box14Mt and R153 largely overestimate the observed extinctions above 24 km. The 3-D simulation "R001 3-D" is superior to all the 2-D simulations, while "R153 3-D" performs worse than the 2-D simulations R001 and R033. Likewise, in June 1992, R001, R010 and R017 also do a better job than other 2-D simulations. The two 3-D simulations "R001 3-D" and "R153 3-D" are now both superior to all 2-D model results, although the differences between them start to shrink as the their aerosol burdens are now within 10% from each other. Here the 3D model shows a better extinction vertical profile likely because the 3D model uses an improved numerical scheme based on Walcek (2000) for sedimentation, while the 2-D model uses an upwind scheme, which would cause artificial upward transport of particles to high altitudes (Benduhn and Lawrence, 2013; Sheng et al., 2015). Evaporation of aerosol becomes important only above ∼32 km, therefore should play a minor role in explaining the discrepancy between the 2-D AER and 3-D SOCOL-AER. Overall, the results from SPARC20Mt, Box14Mt, R033 and R153 display a common deficiency, as they tend to overestimate aerosol extinctions in high altitudes above 24 km. Excessive mass loading (as in SPARC20Mt or R033) is one of the reasons. However, the shape of the initial mass vertical profiles appears to be at least as important as the initial mass loading. Box14Mt has 30% less total mass loading than SPARC20Mt, but it shows even higher extinctions in high altitudes because it has 40% of its mass injected above 24 km, while SPARC20Mt has only about 20% of its mass there.

Figure 6 compares the modeled aerosol optical thickness (AOT) with the SAGE II measurements. The southward transport of the volcanic clouds observed by SAGE II is reasonably reproduced by the models. The best scenarios here are R001 and R010, whose SO_2 injection profiles peak between 18-21 km and disperse the volcanic plume broadly ($\sigma = 4$ km). In contrast, R017 with a narrow dispersion ($\sigma = 2$ km) constricts the initial SO_2 between 18-22 km, which leads to a faster decay of AOT than R001 and R010. R153 and SPARC20Mt distribute too many aerosols to high latitudes due to injecting SO_2 excessively above 24 km. The impact of the initial SO_2 vertical profile on the hemispheric dispersion of the volcanic clouds is more pronounced in the 3D simulations as shown in the two bottom panels. These results show that spatiotemporal distribution of the volcanic aerosols is affected by initial injection profile of SO_2 and the optimal parameters found in Table 1 would lead to better model results when compared to SAGE II observations.

4 Conclusions

We have conducted over 300 Pinatubo-like simulations by perturbing four parameters which determine the magnitude and vertical distribution of injected SO_2. Our simulations show that the initial SO_2 magnitude and distribution play a significant role in the evolution of stratospheric aerosol properties following the Pinatubo eruption, including rates of poleward transport of volcanic clouds. Our ensemble study suggests that Pinatubo injected less than 17 Mt of SO_2 into the stratosphere, and that good agreement can be reached with a 14 Mt injection. The vertical profile of the injected SO_2 is likely skewed towards the lower stratosphere, with 80% of the SO_2 mass injected below 24 km and the distribution peak likely between 18 and 21 km. We have found a set of initial injection parameters such that the resulting model

simulations fairly reproduce the evolution of stratospheric aerosol properties when compared to HIRS and SAGE II based data. This reduces the uncertainties in modeling the initial sulfur mass loading of Pinabuto.

Acknowledgements. This work was stimulated by the "Assessment of Stratospheric Aerosol Properties (ASAP)", a previous activity of SPARC (Stratosphere-troposphere Processes and their Role in Climate). We thank Jason English and Anthony Baran for helpful discussion on HIRS measurements. We thank Laura Revell and Andrew Gettelman for useful suggestions on our work. We are particularly grateful to Mian Chin for valuable comments which helped to improve the manuscript. Thanks also to the unknown reviewers for their valuable comments. This work was supported by the Swiss National Science Foundation under the grant 200021-130478(IASSA).

References

Aquila, V., Oman, L. D., Stolarski, R. S., Colarco, P. R., and Newman, P. A.: Dispersion of the volcanic sulfate cloud from a Mount Pinatubo–like eruption, Journal of Geophysical Research: Atmospheres, 117, n/a–n/a, doi:10.1029/2011JD016968, http://onlinelibrary.wiley.com/doi/10.1029/2011JD016968/abstract, 2012.

Arfeuille, F., Luo, B. P., Heckendorn, P., Weisenstein, D., Sheng, J. X., Rozanov, E., Schraner, M., Brönnimann, S., Thomason, L. W., and Peter, T.: Modeling the stratospheric warming following the Mt. Pinatubo eruption: uncertainties in aerosol extinctions, Atmos. Chem. Phys., 13, 11 221–11 234, doi:10.5194/acp-13-11221-2013, http://www.atmos-chem-phys.net/13/11221/2013/, 2013.

Azzalini, A.: The Skew-normal Distribution and Related Multivariate Families, Scandinavian Journal of Statistics, 32, 159–188, doi:10.1111/j.1467-9469.2005.00426.x, 2005.

Baran, A. J. and Foot, J. S.: New application of the operational sounder HIRS in determining a climatology of sulphuric acid aerosol from the Pinatubo eruption, Journal of Geophysical Research: Atmospheres, 99, 25 673–25 679, doi:10.1029/94JD02044, http://onlinelibrary.wiley.com/doi/10.1029/94JD02044/abstract, 1994.

Benduhn, F. and Lawrence, M. G.: An investigation of the role of sedimentation for stratospheric solar radiation management, Journal of Geophysical Research: Atmospheres, 118, 7905–7921, doi:10.1002/jgrd.50622, http://onlinelibrary.wiley.com/doi/10.1002/jgrd.50622/abstract, 2013.

Bluth, G. J. S., Doiron, S. D., Schnetzler, C. C., Krueger, A. J., and Walter, L. S.: Global tracking of the SO_2 clouds from the June, 1991 Mount Pinatubo eruptions, Geophysical Research Letters, 19, 151–154, doi:10.1029/91GL02792, http://onlinelibrary.wiley.com/doi/10.1029/91GL02792/abstract, 1992.

Crutzen, P. J.: Albedo Enhancement by Stratospheric Sulfur Injections: A Contribution to Resolve a Policy Dilemma?, Climatic Change, 77, 211–220, doi:10.1007/s10584-006-9101-y, http://link.springer.com/article/10.1007/s10584-006-9101-y, 2006.

Deshler, T.: A review of global stratospheric aerosol: Measurements, importance, life cycle, and local stratospheric aerosol, Atmospheric Research, 90, 223–232, doi:10.1016/j.atmosres.2008.03.016, http://www.sciencedirect.com/science/article/pii/S0169809508000598, 2008.

Deshler, T., Hervig, M. E., Hofmann, D. J., Rosen, J. M., and Liley, J. B.: Thirty years of in situ stratospheric aerosol size distribution measurements from Laramie, Wyoming (41°N), using balloon-borne instruments, Journal of Geophysical Research: Atmospheres, 108, n/a–n/a, doi:10.1029/2002JD002514, http://onlinelibrary.wiley.com/doi/10.1029/2002JD002514/abstract, 2003.

Dhomse, S. S., Emmerson, K. M., Mann, G. W., Bellouin, N., Carslaw, K. S., Chipperfield, M. P., Hommel, R., Abraham, N. L., Telford, P., Braesicke, P., Dalvi, M., Johnson, C. E., O'Connor, F., Morgenstern, O., Pyle, J. A., Deshler, T., Zawodny, J. M., and Thomason, L. W.: Aerosol microphysics simulations of the Mt. Pinatubo eruption with the UKCA composition-climate model, Atmos. Chem. Phys. Discuss., 14, 2799–2855, doi:10.5194/acpd-14-2799-2014, http://www.atmos-chem-phys-discuss.net/14/2799/2014/, 2014.

Dutton, E. G. and Christy, J. R.: Solar radiative forcing at selected locations and evidence for global lower tropospheric cooling following the eruptions of El Chichón and Pinatubo, Geophysical Research Letters, 19, 2313–2316, doi:10.1029/92GL02495, http://onlinelibrary.wiley.com/doi/10.1029/92GL02495/abstract, 1992.

English, J. M., Toon, O. B., and Mills, M. J.: Microphysical simulations of large volcanic eruptions: Pinatubo and Toba, Journal of Geophysical Research: Atmospheres, 118, 1880–1895, doi:10.1002/jgrd.50196, http://onlinelibrary.wiley.com/doi/10.1002/jgrd.50196/abstract, 2013.

Fero, J., Carey, S. N., and Merrill, J. T.: Simulating the dispersal of tephra from the 1991 Pinatubo eruption: Implications for the formation of widespread ash layers, Journal of Volcanology and Geothermal Research, 186, 120–131, doi:10.1016/j.jvolgeores.2009.03.011, http://www.sciencedirect.com/science/article/pii/S0377027309001565, 2009.

Fleming, E. L., Jackman, C. H., Stolarski, R. S., and Considine, D. B.: Simulation of stratospheric tracers using an improved empirically based two-dimensional model transport formulation, Journal of Geophysical Research: Atmospheres, 104, 23 911–23 934, doi:10.1029/1999JD900332, http://onlinelibrary.wiley.com/doi/10.1029/1999JD900332/abstract, 1999.

Guo, S., Bluth, G. J. S., Rose, W. I., Watson, I. M., and Prata, A. J.: Re-evaluation of SO2 release of the 15 June 1991 Pinatubo eruption using ultraviolet and infrared satellite sensors, Geochemistry, Geophysics, Geosystems, 5, n/a–n/a, doi:10.1029/2003GC000654, http://onlinelibrary.wiley.com/doi/10.1029/2003GC000654/abstract, 2004.

Heckendorn, P., Weisenstein, D., Fueglistaler, S., Luo, B. P., Rozanov, E., Schraner, M., Thomason, L. W., and Peter, T.: The impact of geoengineering aerosols on stratospheric temperature and ozone, Environmental Research Letters, 4, 045 108, doi:10.1088/1748-9326/4/4/045108, http://iopscience.iop.org/1748-9326/4/4/045108, 2009.

Herzog, M. and Graf, H.-F.: Applying the three-dimensional model ATHAM to volcanic plumes: Dynamic of large coignimbrite eruptions and associated injection heights for volcanic gases, Geophysical Research Letters, 37, L19 807, doi:10.1029/2010GL044986, http://onlinelibrary.wiley.com/doi/10.1029/2010GL044986/abstract, 2010.

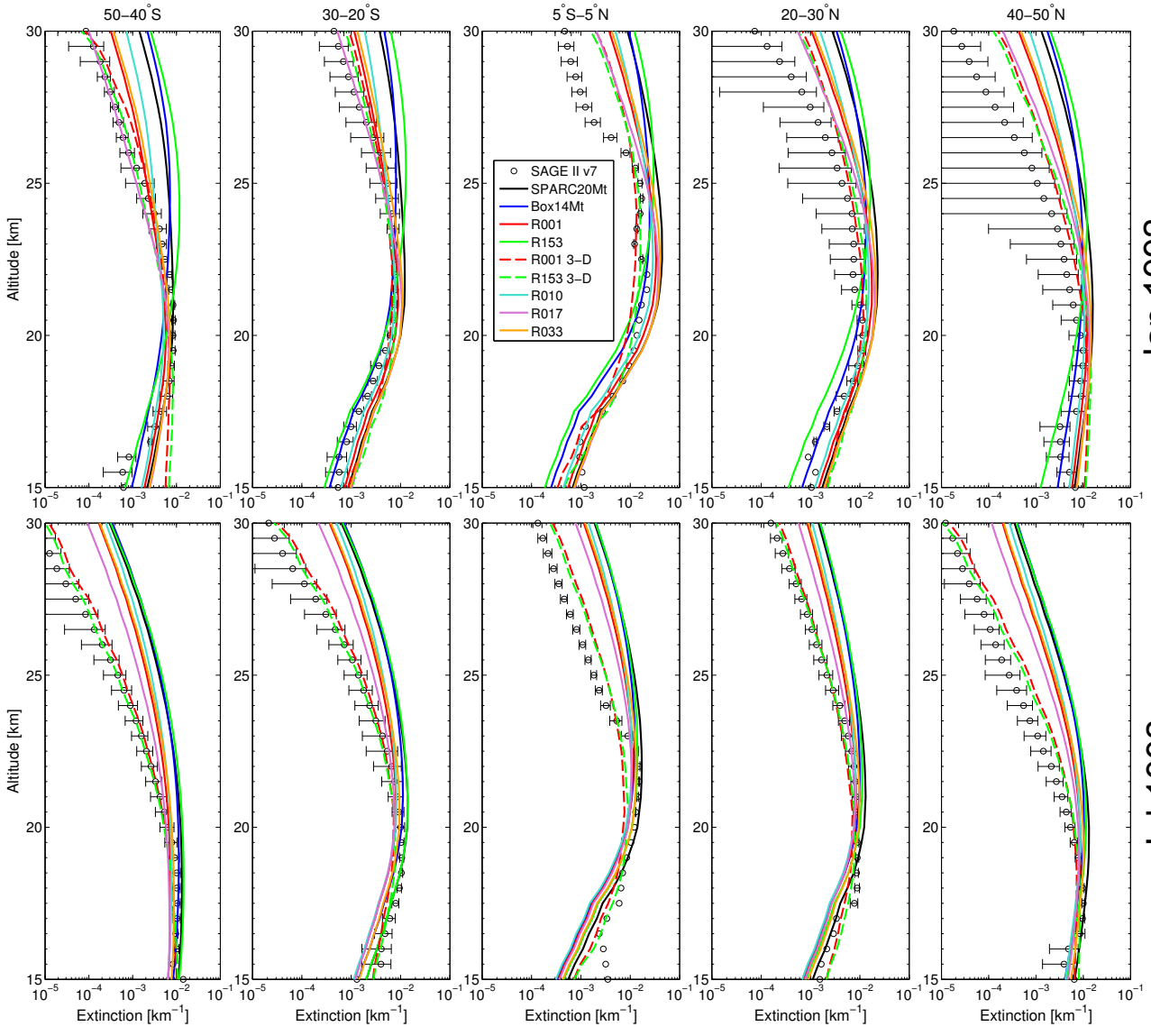

Fig. 5. Aerosol 1020 nm extinction comparisons of SAGE II (version 7.0) and model simulations in five latitude bands (from left to right) 50-40°S, 30-20°S, 5°S-5°N, 20-30°N and 40-50°N for January (upper panel) and July 1992 (lower panel). Solid curves: AER 2-D model results. Dashed curves: 3-D SOCOL-AER model results. Symbols with horizontal bars: SAGE II extinction measurements with bars indicating natural variability (namely observed zonal differences). Symbols without horizontal bars: data from individual ground-based lidar stations used within SAGE-4λ under conditions when the atmosphere was so opaque that SAGE II could not measure, so-called gap-filled data with large uncertainty (SPARC, 2006; Luo, 2015)

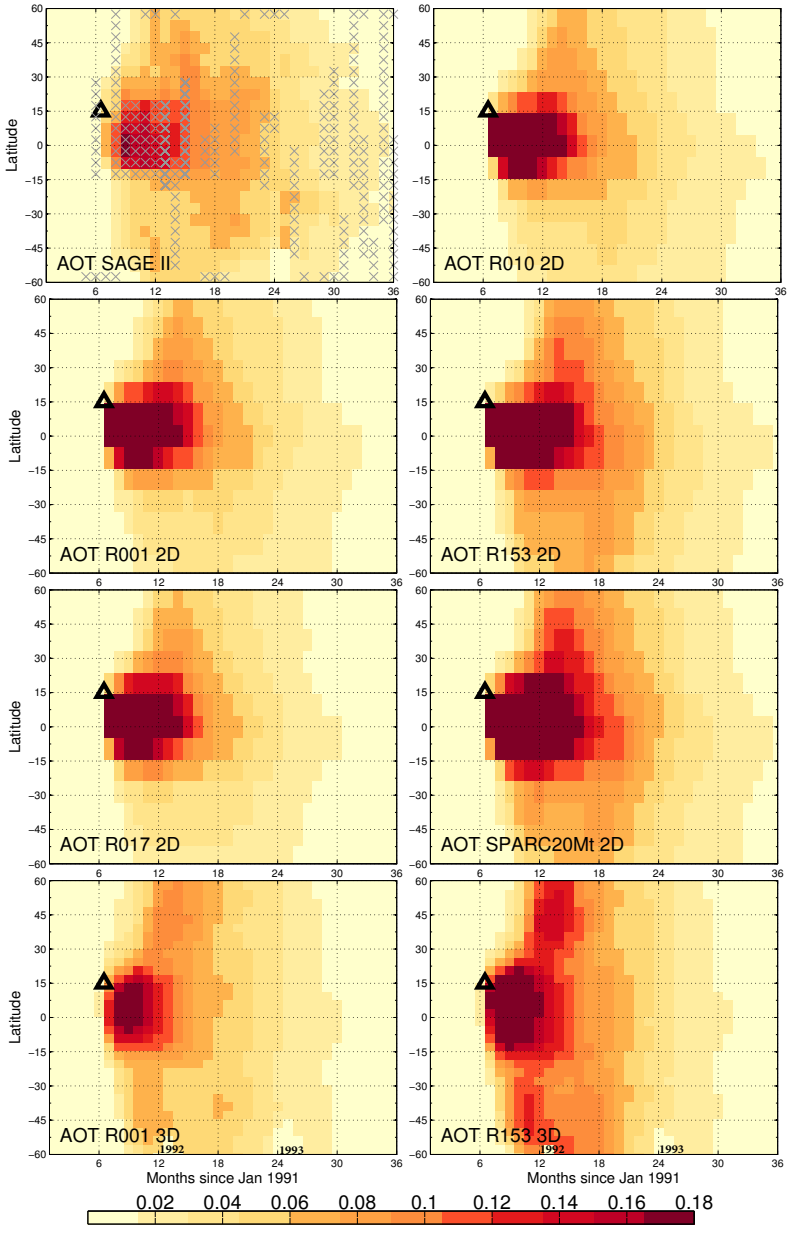

Fig. 6. Aerosol optical thickness (AOT, 15-30 km) comparison between SAGE-4λ and model simulations. Marked regions in AOT SAGE II include gap-filled data. Triangle: time-latitude location of the Pinatubo eruption.

Krueger, A. J., Walter, L. S., Bhartia, P. K., Schnetzler, C. C., Krotkov, N. A., Sprod, I., and Bluth, G. J. S.: Volcanic sulfur dioxide measurements from the total ozone mapping spectrometer instruments, Journal of Geophysical Research: Atmospheres, 100, 14 057–14 076, doi:10.1029/95JD01222, http://onlinelibrary.wiley.com/doi/10.1029/95JD01222/abstract, 1995.

Luo, B. P.: CCMI Aerosol Data - Release Version 2, ftp://iacftp.ethz.ch/pub_read/luo/ccmi/, 2015.

McCormick, M. P., Thomason, L. W., and Trepte, C. R.: Atmospheric effects of the Mt Pinatubo eruption, Nature, 373, 399–404, doi:10.1038/373399a0, http://www.nature.com/nature/journal/v373/n6513/abs/373399a0.html, 1995.

Niemeier, U., Timmreck, C., Graf, H.-F., Kinne, S., Rast, S., and Self, S.: Initial fate of fine ash and sulfur from large volcanic eruptions, Atmos. Chem. Phys., 9, 9043–9057, doi:10.5194/acp-9-9043-2009, http://www.atmos-chem-phys.net/9/9043/2009/, 2009.

Notholt, J., Luo, B. P., Fueglistaler, S., Weisenstein, D., Rex, M., Lawrence, M. G., Bingemer, H., Wohltmann, I., Corti, T., Warneke, T., von Kuhlmann, R., and Peter, T.: Influence of tropospheric SO2 emissions on particle formation and the stratospheric humidity, Geophysical Research Letters, 32, n/a–n/a, doi:10.1029/2004GL022159, http://onlinelibrary.wiley.com/doi/10.1029/2004GL022159/abstract, 2005.

Prinn, R. G., Huang, J., Weiss, R. F., Cunnold, D. M., Fraser, P. J., Simmonds, P. G., McCulloch, A., Harth, C., Reimann, S., Salameh, P., O'Doherty, S., Wang, R. H. J., Porter, L. W., Miller, B. R., and Krummel, P. B.: Evidence for variability of atmospheric hydroxyl radicals over the past quarter century, Geophysical Research Letters, 32, L07 809, doi:10.1029/2004GL022228, http://onlinelibrary.wiley.com/doi/10.1029/2004GL022228/abstract, 2005.

Read, W. G., Froidevaux, L., and Waters, J. W.: Microwave limb sounder measurement of stratospheric SO2 from the Mt. Pinatubo Volcano, Geophysical Research Letters, 20, 1299–1302, doi:10.1029/93GL00831, http://onlinelibrary.wiley.com/doi/10.1029/93GL00831/abstract, 1993.

Robock, A., MacMartin, D. G., Duren, R., and Christensen, M. W.: Studying geoengineering with natural and anthropogenic analogs, Climatic Change, 121, 445–458, doi:10.1007/s10584-013-0777-5, http://link.springer.com/article/10.1007/s10584-013-0777-5, 2013.

Russell, P. B., Livingston, J. M., Pueschel, R. F., Bauman, J. J., Pollack, J. B., Brooks, S. L., Hamill, P., Thomason, L. W., Stowe, L. L., Deshler, T., Dutton, E. G., and Bergstrom, R. W.: Global to microscale evolution of the Pinatubo volcanic aerosol derived from diverse measurements and analyses, Journal of Geophysical Research: Atmospheres, 101, 18 745–18 763, doi:10.1029/96JD01162, http://onlinelibrary.wiley.com/doi/10.1029/96JD01162/abstract, 1996.

Sander, S., Abbatt, J., Barker, J., Burkholder, J., Friedl, R., Golden, D., Huie, R., Kolb, C., Kurylo, M., Moortgat, G., Orkin, V., and Wine, P.: Chemical Kinetics and Photochemical Data for Use in Atmospheric Studies, Evaluation No. 17, JPL Publication 10-6, Jet Propulsion Laboratory, Pasadena, 2011.

Sheng, J.-X., Weisenstein, D. K., Luo, B.-P., Rozanov, E., Stenke, A., Anet, J., Bingemer, H., and Peter, T.: Global atmospheric sulfur budget under volcanically quiescent conditions: Aerosol-chemistry-climate model predictions and validation, J. Geophys. Res. Atmos., 120, 2014JD021 985, doi:10.1002/2014JD021985, http://onlinelibrary.wiley.com/doi/10.1002/2014JD021985/abstract, 2015.

SPARC: SPARC Report No. 4, Assessment of Stratospheric Aerosol Properties (ASAP), WCRP-124 WMO/TD No. 1295, SPARC Report No. 4, edited by: Thomason, L. and Peter, Th., WMO, 2006.

Stenke, A., Schraner, M., Rozanov, E., Egorova, T., Luo, B., and Peter, T.: The SOCOL version 3.0 chemistry–climate model: description, evaluation, and implications from an advanced transport algorithm, Geoscientific Model Development, 6, 1407–1427, doi:10.5194/gmd-6-1407-2013, http://www.geosci-model-dev.net/6/1407/2013/gmd-6-1407-2013.html, 2013.

Stowe, L. L., Carey, R. M., and Pellegrino, P. P.: Monitoring the Mt. Pinatubo aerosol layer with NOAA/11 AVHRR data, Geophysical Research Letters, 19, 159–162, doi:10.1029/91GL02958, http://onlinelibrary.wiley.com/doi/10.1029/91GL02958/abstract, 1992.

Tabazadeh, A., Toon, O. B., Clegg, S. L., and Hamill, P.: A new parameterization of H_2SO_4/H_2O aerosol composition: Atmospheric implications, Geophysical Research Letters, 24, 1931–1934, doi:10.1029/97GL01879, http://onlinelibrary.wiley.com/doi/10.1029/97GL01879/abstract, 1997.

Thomason, L. W., Poole, L. R., and Deshler, T.: A global climatology of stratospheric aerosol surface area density deduced from Stratospheric Aerosol and Gas Experiment II measurements: 1984–1994, Journal of Geophysical Research: Atmospheres, 102, 8967–8976, doi:10.1029/96JD02962, http://onlinelibrary.wiley.com/doi/10.1029/96JD02962/abstract, 1997.

Thomason, L. W., Burton, S. P., Luo, B.-P., and Peter, T.: SAGE II measurements of stratospheric aerosol properties at non-volcanic levels, Atmos. Chem. Phys., 8, 983–995, doi:10.5194/acp-8-983-2008, http://www.atmos-chem-phys.net/8/983/2008/, 2008.

Timmreck, C., Graf, H.-F., and Feichter, J.: Simulation of Mt. Pinatubo Volcanic Aerosol with the Hamburg Climate Model ECHAM4, Theoretical and Applied Climatology, 62, 85–108, doi:10.1007/s007040050076, http://link.springer.com/article/10.1007/s007040050076, 1999.

Toohey, M., Krüger, K., Niemeier, U., and Timmreck, C.: The influence of eruption season on the global aerosol evolution and radiative impact of tropical volcanic eruptions, Atmos. Chem. Phys., 11, 12 351–12 367, doi:10.5194/acp-11-12351-2011, http://www.atmos-chem-phys.net/11/12351/2011/, 2011.

Walcek, C. J.: Minor flux adjustment near mixing ratio extremes for simplified yet highly accurate monotonic calculation of tracer advection, Journal of Geophysical Research: Atmospheres, 105, 9335–9348, doi:10.1029/1999JD901142, http://onlinelibrary.wiley.com/doi/10.1029/1999JD901142/abstract, 2000.

Weisenstein, D. K., Yue, G. K., Ko, M. K. W., Sze, N.-D., Rodriguez, J. M., and Scott, C. J.: A two-dimensional model of sulfur species and aerosols, Journal of Geophysical Research, 102, 13 019–13,035, doi:10.1029/97JD00901, http://www.agu.org/pubs/crossref/1997/97JD00901.shtml, 1997.

Weisenstein, D. K., Penner, J. E., Herzog, M., and Liu, X.: Global 2-D intercomparison of sectional and modal aerosol modules, Atmos. Chem. Phys., 7, 2339–2355, doi:10.5194/acp-7-2339-2007, http://www.atmos-chem-phys.net/7/2339/2007/, 2007.